Interfacial free energy of hard-sphere fluids and solids near a hard wall

Martin Heni and Hartmut Löwen
Institut für Theoretische Physik II, Heinrich-Heine-Universität Düsseldorf, Universitätsstraße 1, D-40225 Düsseldorf, Germany
(Received 17 June 1999)

A hard-sphere system near a planar structureless hard wall is considered in thermodynamic equilibrium. The associated interfacial free energies are calculated both for a bulk fluid and a bulk face-centered-cubic crystal along (111), (110), and (100) orientation. Combining Monte Carlo simulations and thermodynamic integration, we obtain the wall-fluid and the wall-solid interfacial free energy over the whole range of possible bulk densities. The ''exact'' computer simulation data are compared to theoretical approximations. For moderate bulk densities, the wall-fluid interfacial free energies compare reasonably well with scaled-particle theory and density functional results. For the wall-crystal interface, we propose a simple analytical cell theory which yields good agreement with our simulation data over the whole range of bulk crystal densities.
[S1063-651X(99)01912-1]

PACS number(s): 68.10.Cr, 68.35.Md, 82.70.Dd

I. INTRODUCTION

Most of the physical properties of a solid or liquid in contact with a substrate such as wetting, spreading, and heterogeneous nucleation, are governed by the interfacial free energies between the substrate and the material [1]. Therefore a microscopic theory of surface tensions is highly desirable in order to predict the wettability of a given substrate for different materials [2]. Clearly, since this quantity depends on the microscopic interactions between the particles both of the substrate and the material, such a theoretical calculation represents a formidable task, in general.

A first step into this direction is performed in the present paper where we calculate equilibrium surface free energies for one specific type of microscopic interactions. We model the interaction between the particles as hard spheres and describe the substrate as a hard structureless planar wall. Our motivation to study this excluded volume model is threefold: First, the model has the advantage of being simple as it is characterized by a single parameter, namely, the bulk packing fraction η. If one wants to achieve a principal understanding for the surface free energies, one should study first a simple model and generalize it later to more realistic interactions. Second, the hard-sphere interaction is actually realized in suspensions of sterically stabilized colloids [3]. In such systems with mesoscopic particles one has the further advantage that real-space methods such as, e.g., confocal microscopy are possible to explore the structure of the bulk and of interfaces directly, see, e.g., Refs. [4–6]. Third, from a more theoretical point of view, many of the atomic interactions can be appropriately mapped onto an effective hard-sphere systems such that a hard-sphere interaction is useful as a reference case [7,8].

The hard-sphere *fluid* near a hard wall is a standard situation which has been studied in numerous publications. Computer simulations for the density profiles are available and theories, in particular density functional approximations of inhomogeneous systems [9,10], have been tested against the simulation data. What is a bit less common is the interfacial free energy γ itself which is harder to extract from the simulation data since it either requires evaluation of the pressure tensor at the wall [11] or thermodynamic integration over a set of simulation runs [12]. Only few density functional studies are available using the weighted density approximation [13] or variants of it [14] and an analytical scaled-particle expression is known [7,15,16]. In this paper we revisit this problem and show that scaled particle theory and density functional theory compare well with the simulation data. However, for high densities close to freezing the published density functional calculation deviates significantly from our simulation data.

The main topic of the present paper concerns a hard-sphere *solid* near a hard wall where much less is known. The associated interfacial free energy γ now depends also on the orientation of the solid with respect to the wall normal. Apart from a density functional study at the melting point [13], no results for γ have been published in the literature. We use Monte Carlo computer simulations to investigate the interface between a hard wall and a hard-sphere crystal. In particular, we obtain the wall-solid surface free energy over the whole range of bulk densities for (111), (110), and (100) orientations. Furthermore we propose a simple solid cell model for this interface resulting in a simple analytical expression for γ which is in good agreement with our simulation data. Our simulation results can be used as benchmark data to test the ability of classical density functional theories of freezing to predict solid interfaces such as the recently developed Rosenfeld approximation [17].

The paper is organized as follows. In Sec. II, the model is introduced. Our computer simulation technique is described in Sec. III. The case of a bulk fluid is discussed in Sec. IV. The cell theory for the solid is proposed in Sec. V and simulation results are presented in Sec. IV. We finally conclude in Sec. VII.

II. MODEL AND DEFINITION OF THE INTERFACIAL FREE ENERGY

We consider N hard spheres with diameter σ in a large volume V at a fixed temperature T. The finite number density of the spheres is $\rho = N/V$ which can conveniently be expressed in terms of the dimensionless packing fraction η

$=\pi\rho\sigma^3/6$. For excluded volume interactions, temperature only sets the energy scale k_BT (k_B denoting Boltzmann's constant) but does not affect phase transitions or structural correlations. Hence the bulk system is completely specified by the packing fraction η. It is well established [18] that the bulk hard-sphere system exhibits a first order freezing transition from a fluid phase into a face-centered-cubic (fcc) crystal [19]. The coexisting densities are $\eta \equiv \eta_f = 0.494$ for the fluid and $\eta \equiv \eta_s = 0.545$ for the solid.

In detail, the center-of-mass positions of the spheres are denoted by $\vec{r}_i = (x_i, y_i, z_i)$ $(i = 1, \ldots, N)$. Two hard spheres i and j interact via the pair potential

$$U_{HS}(\vec{r}_i, \vec{r}_j) = \begin{cases} \infty & \text{if } |\vec{r}_i - \vec{r}_j| < \sigma \\ 0 & \text{elsewhere} \end{cases}, \tag{1}$$

In the following we include a surface in the hard sphere system. The presence of such a wall is described by an additional external potential

$$W(z_i) = \begin{cases} 0 & |z_i| > \sigma/2, \\ w(z_i) & \text{elsewhere} \end{cases} \tag{2}$$

which acts on the centers of the ith hard sphere ($i = 1, \ldots, N$). For sake of convenience the wall position is at $z = 0$ in a plane parallel to the x-y plane. The actual wall area is A. Although we have a hard impenetrable wall in mind we keep the description a bit more general by allowing also penetrable wall potentials where the function $w(z)$ is finite. For symmetry reasons, $w(z)$ should be an even function, i.e., $w(-z) = w(z)$. The bulk system is recovered for a vanishing $w(z)$ while a hard wall is described by $w(z) \to \infty$. The total potential energy of the system is

$$U(\{\vec{r}_k\}) = \sum_{i=0}^{N} W(z_i) + \sum_{i,j=1;i<l}^{N} U_{HS}(\vec{r}_i, \vec{r}_j) \tag{3}$$

resulting in the canonical partition function

$$Q(N,V,A,T) = \frac{1}{\Lambda^{3N} N!} \int d^3 r_1 \cdots \int d^3 r_N e^{-\beta U(\{\vec{r}_k\})}, \tag{4}$$

where $\{\vec{r}_k\} = (\vec{r}_1, \ldots, \vec{r}_N)$, $\beta = 1/(k_BT)$ and Λ being the (irrelevant) thermal wavelength. The canonical free energy is finally gained as $F(N,V,A,T) = -k_BT \ln Q(N,V,A,T)$.

In the bulk case ($w(z) \equiv 0$), there is no dependence on the area A. Hence we can simply write $F(N,V,A,T) = k_BT\tilde{F}_{\text{bulk}}(\eta)$ where $\tilde{F}_{\text{bulk}}$ is a dimensionless quantity. Introducing a wall of area A adds A as additional thermodynamical variable. In leading order, the full free energy splits into a bulk and a surface contribution [10] $F(N,V,A,T) = k_BT\tilde{F}_{\text{bulk}}(\eta) + \gamma(\eta,T)A + O(L)$ where $\gamma(\eta,T)$ is the interfacial free energy of the system and L is a typical edge length of the system. In other words, the interfacial free energy is the excess free energy per area

$$\gamma(\eta,T) = \frac{F(N,V,T,A) - k_BT\tilde{F}_{\text{bulk}}(\eta)}{A} \tag{5}$$

and can equivalently defined via

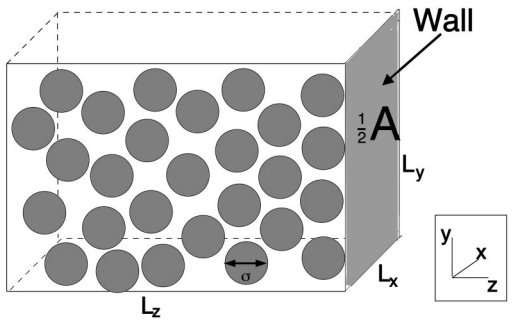

FIG. 1. Geometry of the hard-sphere system under consideration. The simulation box has a volume $V = L_xL_yL_z$ and contains N particles of diameter σ. The total hard-sphere-system–hard-wall-contact area is $A = 2L_xL_y$.

$$\gamma = \left.\frac{\partial F(N,V,T,A)}{\partial A}\right|_{N,V,T}. \tag{6}$$

We finally note that for a hard wall $\gamma(\eta,T) = k_BT\tilde{\gamma}(\eta)$ such that the only nontrivial dependence is on the bulk packing fraction. A suitable reduced quantity is $\gamma^*(\eta) = \tilde{\gamma}(\eta)\sigma^2$. It is this target quantity which we calculate and discuss in the sequel over the whole range of packing fractions both in the fluid and crystalline bulk phase. In the nonhomogeneous crystalline phase, the interfacial free energy γ^* will additionally depend on the orientation of the solid with respect to the wall. Of course, due to thermodynamic stability, γ^* has to be positive.

III. COMPUTER SIMULATION TECHNIQUE

We simulate the hard-sphere fluid and the hard-sphere crystal using a rectangular simulation box of size $V = L_xL_yL_z$ with periodic boundary conditions in all directions. Moreover we can add any given wall potential $W(z)$ according to Eq. (2) to the system. The total surface area of the simulation box is then $A = 2L_xL_y$ since in our setup any single wall applied to the system will appear doubled at both ends of the simulation cell, see Fig. 1. We use standard NVT Monte Carlo (MC) simulation techniques [20,21] keeping the volume and the particle number of the system fixed.

NVT simulations have the advantage of being easily implemented, but bear the disadvantage that artificial stress is introduced in a hard-sphere crystal when inserting a wall. In order to check this we have also performed constant pressure simulations (NPT) [20]. In this case an external pressure is applied perpendicular to the walls which are freely moving otherwise. This allows the system to compensate internal stress. Within the statistical uncertainties both setups yield the same interfacial tensions up to high densities of about $\eta \approx 0.66$ which shows *a posteriori* that the system size in our NVT simulation was large enough. For even higher densities the stress introduced in the NVT simulation is responsible for the slight differences and NPT simulation prove to be more suitable.

During the simulation particular attention has to be paid to the equilibration time especially for dense systems. Furthermore the size of the system in z direction, i.e., perpendicular to the wall has to be fairly large to avoid capillary

effects and other spurious mutual influences of the two walls. Moreover we need large surface areas to exclude line effects. System sizes of about 500–2000 particles yielding surface areas $A/2$ of about $30-60\sigma^2$ and an extension into the z direction of about $L_z=30-40\sigma$ has been used during our simulations. In order to avoid lateral compressional strains in the crystal, the length L_x and L_y where adjusted to the given crystallographic orientation such that a laterally periodic bulk crystal fits exactly into the simulation box.

To get access to the interfacial free energy, there are basically two routes to follow. One can use microscopic relations relating the pressure tensor to the interfacial free energy [11]. This has the advantage of needing less computer runs but requires exact knowledge of the density and the one-particle correlation functions at contact. Extrapolating these quantities with high precision is extremely difficult, as they change rapidly near contact for high densities. We therefore choose another method namely *thermodynamic integration* [12], which gives the free energy of the simulated system with respect to that of a known reference system. From the free energy difference of the system with wall compared to the bulk system we can calculate the surface energy directly from Eq. (5). To compute γ^*, this method requires a whole set of simulations but is still applicable for high densities.

Applying the technique of thermodynamic integration, we start from the known bulk hard-sphere system and insert a gradually increasing wall potential, i.e., we simulate a less and less penetrable wall. The wall potential $W(z)\equiv W(z;\lambda)$ is parametrized with a parameter λ which is chosen to give no wall for $\lambda=0$, a less and less penetrable wall for increasing λ and finally a hard wall for $\lambda\to\infty$. Different wall potentials $w(z;\lambda)$ or the details of the switching on procedure do not change the final result for the free energy and interfacial free energy as long as a reversible integration path is followed. The details of the parametrization, however, will influence the equilibration time and the accuracy of the numerical integration. For the fluid we found the square potential $w(z;\lambda)=\lambda$ sufficient for the thermodynamical integrations. A better choice of the parametrization is a triangular potential $w(z;\lambda)=2\lambda(1-2|z|/\sigma)$ which leads to a quicker equilibration and a smoother integrand especially for a bulk solid. For consistency, we have checked that both parametrizations lead to the same final result.

Let us now sketch the scheme of thermodynamic integration in more detail: To integrate the free energy we need its derivative with respect to the integration parameter λ. This quantity can be written as a statistical average and is thus directly accessible by computer simulations. Consequently,

$$\begin{aligned}\left.\frac{\partial F}{\partial\lambda}\right|_{NVAT} &= -k_BT\frac{1}{Q}\left.\frac{\partial Q}{\partial\lambda}\right|_{NVAT}\\ &= \frac{1}{Q}\frac{1}{\Lambda^{3N}N!}\int d^3r_1\cdots\int d^3r_N\frac{\partial W(z;\lambda)}{\partial\lambda}\\ &\quad\times\exp^{-\beta U(\{\vec{r}\};\lambda)}\\ &= \left\langle\frac{\partial W(z;\lambda)}{\partial\lambda}\right\rangle_\lambda,\end{aligned}\tag{7}$$

where $\langle\cdots\rangle_\lambda$ denotes a canonical average with a penetrable wall. A typical example of the integrand $\langle\partial W(z;\lambda)/\partial\lambda\rangle_\lambda$ of the thermodynamical integration is shown in Fig. 2 for a triangular potential. One sees that typically 10–20 integration points are necessary. For large λ, the integrand could be well fitted by an algebraic decay $\propto\lambda^{-2}$ which was used to estimate the tail of the integrand. The integrand $\langle\partial W(z;\lambda)/\partial\lambda\rangle_\lambda$ is positive which implies that the interfacial tension for a penetrable wall is smaller than that for a hard wall.

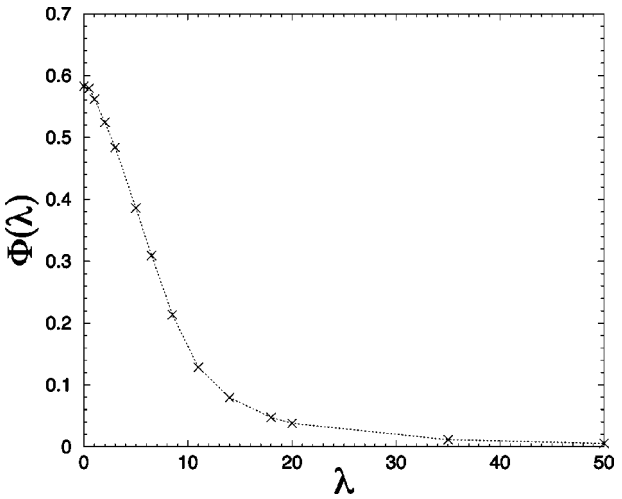

FIG. 2. Integrand $\Phi(\lambda):=\langle\partial W(z;\lambda)/\partial\lambda\rangle_\lambda/(k_BT)$ as dimensionless quantity vs λ for a hard-sphere fcc crystal at $\eta=0.63$ in (111) orientation using a triangular wall potential.

Using Eq. (5) the interfacial free energy γ of the system with a hard wall can be written as

$$\gamma=\frac{\int_0^\infty d\lambda\left\langle\frac{\partial W(z;\lambda)}{\partial\lambda}\right\rangle_\lambda}{A}.\tag{8}$$

We used different system sizes and surface areas to estimate the statistical and finite size errors in the calculation. Within the different system sizes used in our simulations, we do not find any systematic corrections. This indicates that our systems are large enough.

IV. HARD-SPHERE FLUID NEAR A HARD WALL

The interfacial tension of a hard-sphere fluid (i.e., $\eta<\eta_f$) at a hard wall can be analytically calculated within scaled-particle theory (SPT) [7,15]. The key quantity of SPT is $\overline{\gamma}\equiv\gamma-P\sigma/2$ (with P being the bulk pressure) which is negative in general. SPT yields

$$\overline{\gamma}_{\mathrm{SPT}}=-k_BT\frac{9}{2\pi\sigma^2}\eta^2\frac{1+\eta}{(1-\eta)^3}.\tag{9}$$

In SPT the bulk pressure is equivalent to the bulk pressure obtained by the Percus-Yevick compressibility equation of state [7]. Therefore remaining inside SPT one has to add

$$P_{PY}\sigma/2=k_BT\frac{6}{\pi}\eta\frac{1+\eta+\eta^2}{(1-\eta)^3}\tag{10}$$

TABLE I. Simulation results for the fluid: Given are the packing fraction η, the interfacial free energy γ^* with its statistical error and number N of particles in the simulation box as well as the maximal surface area $A/2$ used in the simulation.

η	γ^*	N	$A/2\sigma^2$
0.100	0.124 ± 0.05	684	59.22
0.200	0.325 ± 0.02	504–1008	49.74
0.300	0.656 ± 0.03	480–1024	50.61
0.400	1.195 ± 0.11	1024	41.78
0.436	1.543 ± 0.08	1024	39.42
0.472	1.726 ± 0.07	1008	28.10
0.490	1.890 ± 0.09	1008–2500	57.02

as bulk pressure in order to get γ_{SPT}. Yet a more accurate alternative is to use the Carnahan-Starling equation of state [22] to obtain the bulk pressure

$$P_{\mathrm{CS}}\sigma/2 = k_B T \frac{6}{\pi}\eta \frac{1+\eta+\eta^2-\eta^3}{(1-\eta)^3}. \tag{11}$$

In the following we will use bulk pressure Eq. (11) to obtain the interfacial free energy $\gamma_{\mathrm{SPT}} = \overline{\gamma}_{\mathrm{SPT}} + P_{\mathrm{CS}}\sigma/2$.

Another theoretical approach to obtain γ is via classical density functional theory (DFT) of inhomogeneous systems. Using different variants of the weighted-density approximation, the interfacial free energy was calculated by Götzelmann *et al.* [14] for moderate densities and by Ohnesorge *et al.* [13] near freezing.

Data for γ from molecular dynamics (MD) simulations were known already for four different densities in Ref. [11]. Moreover Ref. [16] uses simulation results to fit the interfacial free energy to an empirical formula for γ.

We have applied our scheme of thermodynamic integration to this problem and obtained further data for γ on a finer density grid and up to higher densities which are given in Table I. All data available are summarized in Fig. 3. The scaled-particle theory is in good agreement with the simulation if the bulk pressure is taken from the Carnahan-Starling equation. DFT provides good data for moderate densities but fails near freezing. We remark that the discrepancies at freezing might be due to the actual approximation used for the density functional.

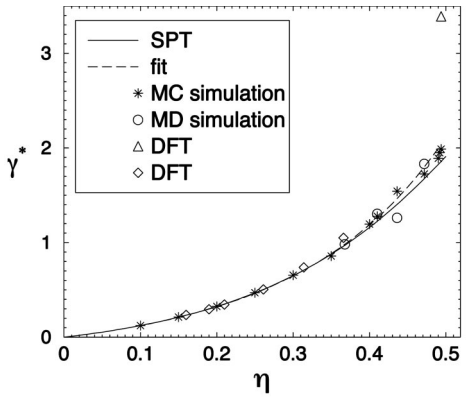

FIG. 3. Reduced interfacial free energy γ^* of the hard-sphere fluid in contact with a hard wall vs packing fraction η. Solid line: scaled-particle theory with Carnahan-Starling equation of state; dashed line: empirical fit from Ref. [16];*: our simulation data; open circle: MD simulation from Ref. [11]; diamonds: DFT from Ref. [14]; triangles: DFT from Ref. [13].

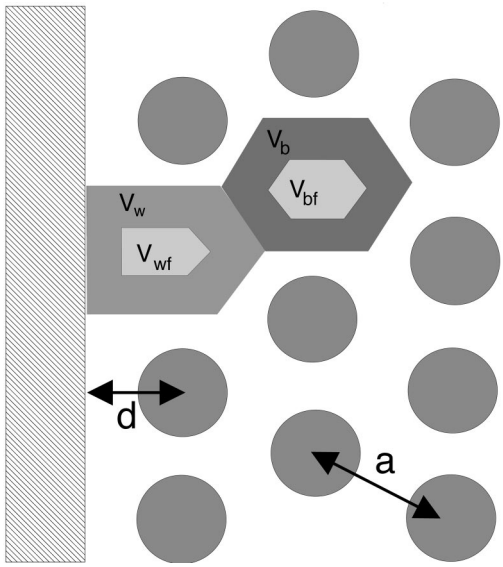

FIG. 4. Two-dimensional hard disk crystal in (11) orientation near the hard wall. The Wigner-Seitz cell volume (resp. area) for a bulk particle V_b and for a wall particle V_w is shown. Inside these cells the free volume cell is indicated as V_{wf} and V_{bf}. The distance of the first layer of particles to the wall is d and the bulk mean particle distance is a.

We finally remark that precrystallization on the hard wall occurs very close to the bulk freezing transition [23]. The thermodynamic integration method, however, is not applicable if a phase transition is crossed along the integration. As is common in any wetting problem, we have hence *extrapolated* the data from lower densities $\eta \approx 0.49$ to the freezing density $\eta_f = 0.494$ to extract the metastable wall-fluid surface tension at freezing. We obtained $\gamma^* = 1.99 \pm 0.18$ which is about 7% above the theoretical value predicted by scaled-particle theory combined with the Carnahan-Starling equation of state.

V. HARD-SPHERE FCC CRYSTAL NEAR A HARD WALL: CELL THEORY

A. General idea

The cell theory (CT) provides a simple analytical estimate of the bulk free energy of the hard-sphere crystal [24]. It was also applied to compute the elastic constants of the hard sphere solid [25] and the location of solid-solid transitions in confining geometry [26]. In the following we shall generalize this concept to extract the interfacial free energy of a hard sphere solid near a hard wall for different orientations. The situation is schematically shown for a two-dimensional hard disk crystal along (11) orientation in Fig. 4.

As there is no major difference between the two- and three-dimensional analysis, we do it in a general spatial dimension D and apply the parameter for the dimensions ($D = 2,3$) later on. Let us first recapitulate the bulk theory: In a given solid lattice, the particles have a bulk mean particle distance a which is the distance between nearest neighbors of

the lattice. We consider the particles to be confined in independent Wigner-Seitz (or Voronoi) cells of the solid. This cell has a volume $V_b = g_b a^D$ where g_b is a geometrical prefactor that depends on the lattice type and on dimensionality D. Each center-of-mass coordinate of the hard spheres can move within a free volume [27] of

$$V_{bf} = g_b (a-\sigma)^D \tag{12}$$

without touching the neighboring spheres. Hence one obtains a lower bound for the bulk partition function, $Q \geqslant (V_{bf}/\Lambda^D)^N$, which provides an upper bound to the bulk free energy

$$F \leqslant -N k_B T \ln\left(\frac{g_b (a-\sigma)^D}{\Lambda^D}\right). \tag{13}$$

This upper bound becomes asymptotically exact for close-packing occurring for $\eta \to \eta_{\mathrm{CP}} = \pi\sqrt{2}/6 = 0.741\cdots$(3D) [27].

We now include a hard wall which induces an inhomogeneity in the problem. We assume that the wall will only influence the first layer of the crystal. This introduces the distance of the center of-mass coordinates in the first layer to the wall as new parameter d, see again Fig. 4. All other layers of the crystal are treated within the bulk-approach. To be specific let us consider first a closed packed orientation, the (111) orientation in 3D, respectively, the (11) orientation in 2D. The form of the Wigner-Seitz cell of the wall particles is different from the bulk. It has a volume

$$V_w = \frac{V_b}{2} + g_w d a^{D-1}, \tag{14}$$

where g_w is a further geometric prefactor depending on the lattice type, the orientation and on D. The free volume accessible for the wall particles is

$$V_{wf} = \frac{V_{bf}}{2} + g_w\left(d - \frac{\sigma}{2}\right)(a-\sigma)^{D-1}. \tag{15}$$

Again we get an upper bound for the free energy within this approach. If one optimizes this bound one gets $V_{bf} = V_{wf}$ [28] which yields

$$d = \frac{g_b}{2g_w}(a-\sigma) + \frac{\sigma}{2} \tag{16}$$

resulting in the same free energy per particle as in the bulk case. The principal difference now, however, is that the mean distance $a = a(N,V,A)$ depends implicitly on the particle number N, the physical total volume V and on the area A. The dependence is explicitly gained by splitting the total volume into a bulk and a surface part

$$\begin{aligned} V &= (N - N_w)V_b + N_w V_w \\ &= N g_b a^D - \frac{A}{g_w a^{D-1}}\left(\frac{g_b}{2}a^D - g_w d a^{D-1}\right) \\ &= N g_b a^D + \sigma A\left(\frac{g_w - g_b}{2g_w}\right), \end{aligned} \tag{17}$$

where $N_w = A/(g_w a^{D-1})$ is the number of particles touching the wall. Equation (17) gives the desired relation $a = a(N,V,A)$. Finally, the interfacial tension is analytically obtained by combining Eq. (13) and (6) as

$$\gamma \equiv \gamma_{\mathrm{CT}} = k_B T \frac{\sigma}{(a-\sigma)a^{D-1}} \frac{1}{2g_w g_b}(g_w - g_b), \tag{18}$$

where a now is the bulk mean particle distance. Different from the bulk theory, γ_{CT} does not provide an upper bound for the exact interfacial tension. Before inserting the appropriate geometric factors for the different crystal orientations we note that this model applies well for fairly close packed surfaces, i.e., crystal orientations in 3D along (111) or even (100) orientation and in 2D along the (11) orientation. For looser packed orientations as the (110) orientation in 3D and the (10) orientation in 2D the calculation becomes more complicated as the free cells and Wigner-Seitz cells of the second layer cannot be neglected anymore. Nevertheless the principles of the cell theory can be applied as well but the calculations become more tedious. We therefore refer to the Appendix for details of the calculations.

Explicitly, for $D=2$ in (11) orientation, $g_b = \sqrt{3}/2$ and $g_w = 1$. Hence Eq. (18) reduces to

$$\gamma_{\mathrm{CT}} \equiv \gamma_{\mathrm{CT}}^{(11)} = k_B T \frac{1}{\sqrt{3}} \frac{\sigma}{(a-\sigma)a}\left(1 - \frac{\sqrt{3}}{2}\right) \tag{19}$$

with the bulk mean particle distance $a = \sigma\sqrt{\pi/2\sqrt{3}\,\eta}$, η denoting the area fraction. In (10) orientation, we can expand the exact solution given in Appendix A to first order and obtain $g_b = \sqrt{3}/2$ and $g_w \approx \sqrt{3}$.

For $D=3$ in (111) orientation, on the other hand, $g_b = 1/\sqrt{2}$ and $g_w = \sqrt{3}/2$ and Eq. (18) yields

$$\gamma_{\mathrm{CT}} \equiv \gamma_{\mathrm{CT}}^{(111)} = k_B T \frac{\sqrt{3}-\sqrt{2}}{\sqrt{3}\sqrt{2}} \frac{\sigma}{(a-\sigma)a^2} \tag{20}$$

with the bulk mean particle distance $a = \sigma(\sqrt{2}\pi/6\eta)^{1/3}$. In (100) orientation, we obtain $g_b = 1/\sqrt{2}$ and $g_w = 1$ and in (110) orientation the first order expansion of the exact solution of the Appendix gives the geometric factor $g_b = 1/\sqrt{2}$ and $g_w \approx \sqrt{2}$.

B. Cell theory with fixed neighbors

The cell theory neglects configurations of collective excursions of neighboring particles from their lattice position. These can be included approximately by keeping all neighbors fixed on their lattice positions. This yields a better free energy for densities away from close-packing and also locates the melting point better than the original CT. Then, of course, the bulk theory is not any longer an upper bound to the exact free energy. This assumption can be directly transferred to the interfacial situation by assuming larger free volume cells. The final result in this cell theory with fixed neighbors (CTFN) is

$$\gamma_{\mathrm{CTFN}} = k_B T \frac{\sigma}{(a-\sigma)a^{D-1}} \frac{1}{g_w g_b}\left(\frac{g_w}{2} - g_b + \frac{g_b}{2}\frac{a}{\sigma}\right) \tag{21}$$

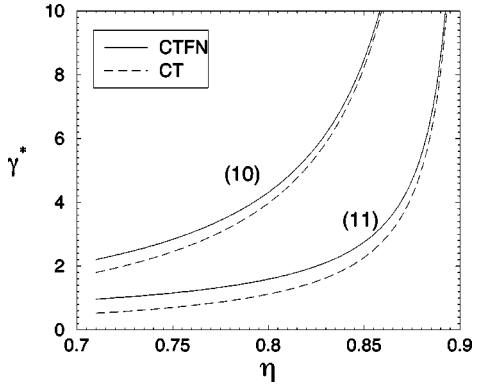

FIG. 5. Reduced interfacial free energy $\gamma^*=\gamma\sigma/(k_BT)$ of a two-dimensional hard disk crystal in contact with a hard line vs bulk area fraction η. Both (11) and (10) orientations are shown for the CT (dashed lines) and the CTFN (solid lines).

which gives for $D=2$ in (11) orientation

$$\gamma_{\mathrm{CTFN}}^{(11)}=k_BT\frac{2}{\sqrt{3}}\frac{\sigma}{(a-\sigma)a}\left(\frac{1}{2}-\frac{\sqrt{3}}{2}+\frac{\sqrt{3}}{4}\frac{a}{\sigma}\right) \tag{22}$$

and for $D=3$ in (111) orientation

$$\gamma_{\mathrm{CTFN}}^{(111)}=k_BT\frac{\sigma}{(a-\sigma)a^2}\left(\frac{1}{\sqrt{2}}-\frac{2}{\sqrt{3}}+\frac{1}{\sqrt{3}}\frac{a}{\sigma}\right). \tag{23}$$

The results for the (10) orientation in 2D and the (100) and (110) orientations in 3D can readily be calculated by inserting the geometric factors from above into Eq. (21). It is intuitively expected that the true interfacial free energy will be bounded by the CT and the CTFN theory and that the CTFN theory will work better than the CT theory.

C. Results in two dimensions

Results within the CT and CTFN theory are displayed for $D=2$ in Fig. 5 for (11) and (10) orientation. A crystal is stable for area fractions between freezing at $\eta_s=0.71$ [29] and close-packing occurring at $\eta_{cp}=\pi/(2\sqrt{3})=0.907\cdots$. The whole stability region of the 2D crystal is shown in Fig. 5. The CTFN gives higher interfacial free energies than the simple CT. Furthermore, the (11) orientation has a significantly lower interfacial free energy than the (10) orientation since a linear chain of disks is better packed along a hard line than a zig-zig structure as realized for the (10) orientation which is rotated about an angle of 30° with respect to the (11) orientation. Clearly, in both cases, γ diverges as close packing is approached.

VI. HARD-SPHERE FCC CRYSTAL NEAR A HARD WALL: SIMULATION RESULTS

A. The interfacial free energy in 3D

Results for γ^* for different orientations and bulk densities are shown in Fig. 6 and collected in Table II. With our choice of the integration parameters we are not yet able to fully equilibrate the systems for densities larger than γ^* ≈ 0.70. A more sophisticated wall insertion and longer computer runs would be needed to extend the simulations beyond these densities.

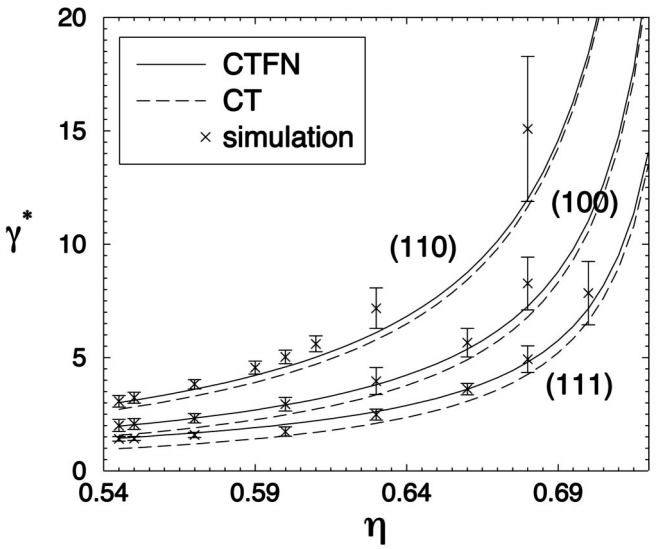

FIG. 6. Reduced interfacial free energy γ^* of a hard-sphere crystal in contact with a hard wall vs bulk packing fraction η. The dashed lines are from CT and the solid lines from CTFN. The crosses are the simulation results. From top to bottom: (110), (100), and (111) orientation.

As becomes evident from Fig. 6 there is good agreement of the simulation data with the simple cell theory over the whole range of packing fractions η. In particular, the CTFN almost perfectly reproduces the simulation data for (111) and (100) orientation. The relative differences between CTFN theory and simulation at freezing ($\eta=0.545$) is less than two percent.

Moreover it is interesting to compare the ratio of the surface tension for different orientations. Simulation data yield a ratio of $\gamma_{110}^*:\gamma_{100}^*:\gamma_{111}^*=2.2:1.4:1.0$ near bulk freezing ($\eta=0.545$) and a ratio of $\gamma_{110}^*:\gamma_{100}^*:\gamma_{111}^*=2.8:1.5:1.0$ for higher bulk densities of $\eta=0.63$. It is appealing to compare these ratios with a picture of broken bonds to nearest neighbors where one gets $\gamma_{110}^*:\gamma_{100}^*:\gamma_{111}^*=2.0:1.3:1.0$ for all densities. Indeed these ratios are very similar for the hard sphere system although there are actually no bonds generated by our interaction potential.

TABLE II. Simulation results for the crystal. Shown are the packing fraction η, the interfacial free energy γ^* for different orientations of the crystal with its statistical error and number N of particles in the simulation box as well as the maximal surface area $A/2$ used in the simulation.

η	$\gamma^*(111)$	$\gamma^*(100)$	$\gamma^*(110)$	N	$A/2\sigma^2$
0.545	1.42±0.10	2.01±0.26	3.08±0.26	504–1500	53.12
0.550	1.43±0.09	2.08±0.24	3.24±0.24	504–1408	33.79
0.570	1.59±0.12	2.32±0.21	3.83±0.21	1024–1408	32.99
0.600	1.74±0.21	2.95±0.30	5.03±0.30	1500	49.82
0.630	2.49±0.24	3.97±0.59	7.18±0.89	504–1408	30.86
0.680	4.93±0.58	8.26±1.16	15.08±3.20	1024	29.33
0.700	7.85±1.40			1024	28.77

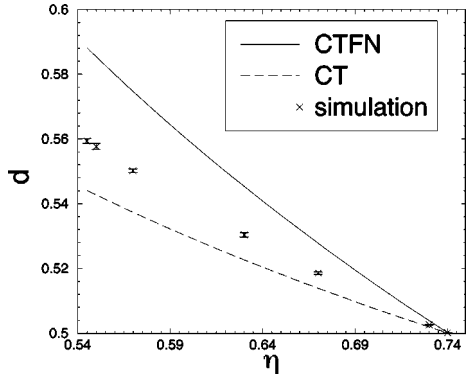

FIG. 7. Reduced distance d^* of the first layer from the wall for fcc (111) orientation vs bulk packing fraction η. The dashed lines are from CT and the solid lines from CTFN. The crosses are the simulation results.

Finally, the interfacial tensions for (110) and (100) orientations are larger than that for (111) orientations. This implies that a solid will pick the (111) orientation which provides most efficient packing near a planar hard wall.

B. Cumulants of the density profile in the first layer

Another important quantity which is the output of any density functional calculation is the inhomogeneous equilibrium one-particle density $\rho(\vec{r})$. Our simple cell theory assumes a homogeneous density distribution within the free cells. We have tested this against computer simulation data. To be specific we introduce cumulants of the density profile within the first adjacent crystalline layer by defining the moments

$$\overline{z^m}=\frac{\int_{-\infty}^{\infty}dx\int_{-\infty}^{\infty}dy\int_0^{z_0}dz z^m\rho(x,y,z)}{\int_{-\infty}^{\infty}dx\int_{-\infty}^{\infty}dy\int_0^{z_0}dz\rho(x,y,z)}, \tag{24}$$

where z_0 denotes the position of the first minimum in the laterally averaged density profile. From this sequence of moments one can deduce several important quantities. First the averaged distance of the first layer from the wall can be gained by $\overline{z}$. We normalize this quantity appropriately by considering $d^*=\overline{z}/\sigma$. The second moment $\overline{z^2}$ is related to the width of the density profiles in z-direction. We define a reduced second cumulant by

$$w^*:=\frac{\sqrt{\overline{z^2}-\overline{z}^2}}{a}. \tag{25}$$

In the bulk system this quantity is proportional to the Lindemann parameter L of the solid describing the root-mean-square displacement around the lattice positions normalized by a. In fact, $w^*=L/\sqrt{3}$. Finally we define the third cumulant (or the reduced skewness) s^* via

$$s^*:=\frac{(\overline{z^3}-3\overline{z^2}\,\overline{z}+2\overline{z}^3)^{1/3}}{\sqrt{\overline{z^2}-\overline{z}^2}}. \tag{26}$$

Obviously, $s^*=0$ in the bulk system due to inflection symmetry.

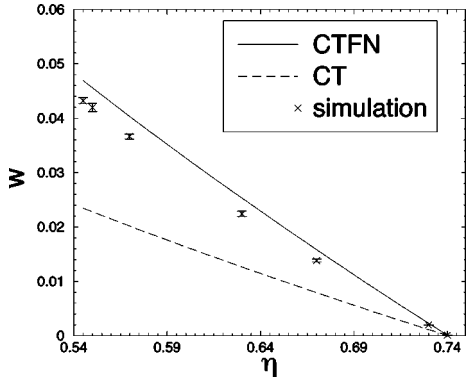

FIG. 8. Same as Fig. 7 but now for the reduced width w^*.

In cell theory the density $\rho(x,y,z)$ is assumed to be smeared out uniformly over the free cell. Hence the moments are directly obtained by integrating over the free cell. In the simulation the density $\rho(x,y,z)$ is readily calculated and used as input into Eq. (24).

Results for the distance d^* of the first layer from the wall are presented in Fig. 7. d^* varies almost linearly with the bulk packing fraction η. The cell theory yields reasonable values as compared to simulation. As close packing is approached, the first layer sticks to the wall, hence $d^*\rightarrow 0.5$ in this limit.

In Fig. 8 we present the reduced width w^* of the first layer versus packing fraction η. The presence of the wall significantly restricts the motion of the particles in the first layer into z direction. This becomes evident by comparing the simulation data with the bulk Lindemann parameter at bulk freezing [30]: The bulk width is 0.074 while the wall results in a strongly reduced width of $w^*=0.043\pm 0.001$. Again the cell theories yield reasonable values and correct trends as compared to the simulation data. The η dependence is again almost linear.

Finally, in Fig. 9, the skewness s^* of the first layer is shown. It is of the order of unity indicating a significant asymmetric density distribution distorted by the wall. The reduced skewness is practically independent of η. The cell theories both underestimate s^* by a factor of one half but also do not exhibit any η dependence. The increasing deviations between cell theory and simulation as the order of the cumulants is growing is due to the fact that the higher mo-

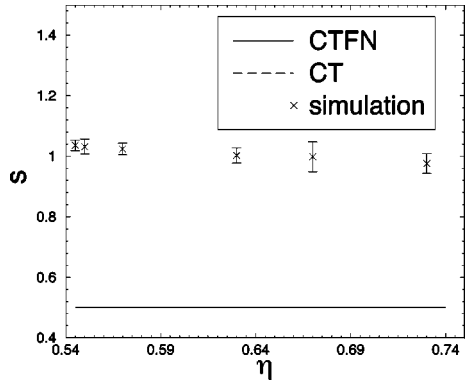

FIG. 9. Same as Fig. 7 but now for the reduced skewness s^*. We note that the CT (dashed line) and CTFN (solid line) fall onto the same curve.

ments are more sensitive to the tail of the distribution. This tail is not correctly described by a sharp-kink density profile as assumed in cell theory. We remark that a better theoretical description of the cumulants can be obtained by density functional calculations. A detailed comparison with our simulation result should provide a stringent test of the current density functional approximations.

VII. CONCLUSIONS

We have calculated the interfacial free energy of a hard-sphere solid near a hard wall and found good agreement with a simple analytical cell theory. Our work demonstrates that the thermodynamic integration method can be applied to surface problems and provides benchmark data to test more elaborate theories.

Let us finally discuss some interesting open questions. First, the equilibrium interfacial free energy between a fluid and a solid at coexistence should be calculated for different orientations. There has been a discussion in the literature [31] about this number which directly influences the nucleation rate of sterically stabilized colloidal suspensions [32–34]. This number will also determine the occurrence of precrystallization [23]. The structure of the interface has been extensively simulated [35–37] but the interfacial tension is still unknown. Second, a structured surface should be investigated. It is expected that the interfacial free energy is reduced considerably if the microscopic surface pattern is compatible with that of the adjacent solid. A peculiar wall structure is a wedge geometry where the structure of the hard sphere fluid has been investigated recently [38]. Furthermore one should simulate the hard disk crystal near a hard line which we did not discuss in our present work. The problem here is that even the nature of the bulk melting transition is controversial [29,39]. Third, for very loosely packed orientations, a faceting transition towards stable vicinal orientations [40] is expected. This should be verified for hard sphere crystals. Finally, the method of thermodynamic integration is also applicable to calculate surface free energies of solid-solid interfaces such as twin boundaries [41] and interfaces between different stacking sequences [42]. Work along these lines is in progress.

ACKNOWLEDGMENTS

We thank M. Dijkstra, B. Evans, R. Roth, M. Schmidt, and M. Watzlawek for helpful remarks. Financial support by the Deutsche Forschungsgemeinschaft via the Schwerpunktsprogramm Benetzung und Strukturbildung an Grenzflächen is gratefully acknowledged.

APPENDIX

The calculation of more open wall structures such as the (10) orientation in 2D or the (110) orientation in 3D is more complicated. The reason is that the crystal layers near the wall are so open that not only the first layer of the crystal is influenced by the wall but also at least the second layer. To find the minimum of the free energy one needs to minimize the position of both layers.

As an approximation, we do not minimize the volume of the Wigner-Seitz cells of the second layer. We include its full volume into the calculation though. This will slightly overestimate the free interfacial energy of the crystal-wall interface.

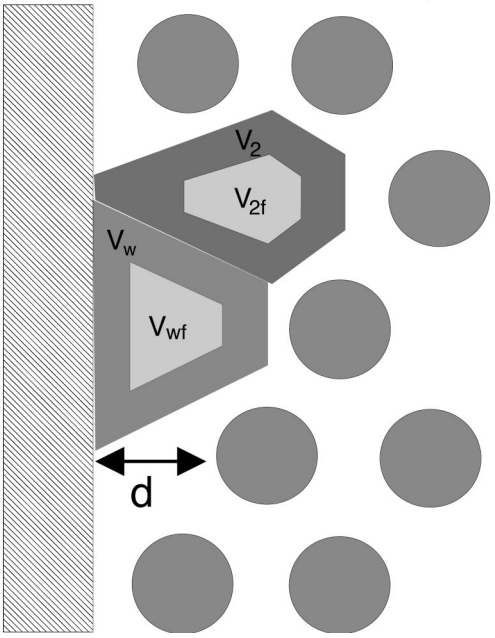

FIG. 10. Same as in Fig. 4 but now for (10) orientation. The distance of the first layer of particles to the wall is d. It can be seen that the effect of the second layer is not negligible.

1. The 2D (10) orientation

For the (10) orientation in 2D we have a free volume of (see Fig. 10)

$$V_{wf}=\frac{V_{bf}}{2}+\left(d-\frac{1}{2}\right)\left(\frac{2\sqrt{3}a}{3}+\frac{\sqrt{2}d}{3}-1\right) \tag{A1}$$

which gives after minimization of the free energy the distance of the first layer as

$$d=\frac{\sqrt{3}}{2}+\frac{1}{4}-a+\frac{1}{4}\sqrt{25-4\sqrt{3}-16\sqrt{3}+28a^2}. \tag{A2}$$

For evaluating the volume change of the system induced by the wall it is necessary to include the volume occupied by the second layer Wigner-Seitz cells into the calculation. The total volume is therefore

$$V=Ng_ba^2+A\left(d-\frac{a}{4}\right) \tag{A3}$$

which can be combined with Eq. (6) to obtain the surface tension

$$\gamma_{\mathrm{CT}}\equiv\gamma_{\mathrm{CT}}^{(10)}=k_BT\frac{1}{2\sqrt{3}}\frac{\sigma}{a(a-\sigma)}(2\sqrt{3}+1-5a+\sqrt{25-4\sqrt{3}-16\sqrt{3}a-16a+28a^2}) \tag{A4}$$

which can be expanded around $a=\sigma$ by the leading term in $\sigma/a(a-\sigma)$ to fit the form of Eq. (18) using a geometric factor of $g_w=\sqrt{3}$.

2. The 3D (110) orientation

In (110) orientation we get a free volume term of

$$V_{wf}=\frac{V_{bf}}{2}+\sqrt{2}\left(d-\frac{1}{2}\right)(a-1)^2-\frac{\sqrt{2}}{24}(a-1)^3+\frac{\sqrt{2}}{3}\left(\frac{a}{2}-d\right)^3. \tag{A5}$$

The minimization of the free energy results in a wall distance of the first layer of

$$d=a\left(c_\alpha+\frac{1}{2}\right)-c_\alpha, \tag{A6}$$

where $c_\alpha=\sqrt{3}\sin\alpha-\cos\alpha$ and $\alpha=\arctan(\sqrt{231}/5)/3$. The total volume is

$$V=Ng_b a^3+A\left(d-\frac{a}{4}\right) \tag{A7}$$

which can be combined with Eq. (6) to obtain the surface tension as

$$\gamma_{\mathrm{CT}}\equiv\gamma_{\mathrm{CT}}^{(110)}=k_BT\frac{\sqrt{2}\sigma}{a^2(a-\sigma)}\left(\frac{ac_\alpha}{\sigma}+\frac{a}{4\sigma}-c_\alpha\right). \tag{A8}$$

Again this can be expanded around $a=\sigma$ by the leading term in $\sigma/a(a-\sigma)$ to fit the form of Eq. (18) by a geometric factor of $g_w=\sqrt{2}$. The expressions for the CTFN can be obtained by the same calculation by assuming the enlarged free volume cells or by inserting the geometric prefactors into Eq. (21).

[1] P. G. de Gennes, Rev. Mod. Phys. **57**, 827 (1985).
[2] S. Dietrich, in *Phase Transitions and Critical Phenomena*, edited by C. Domb and J. L. Lebowitz (London, Academic Press, 1988), Vol. 12, pp. 1–128.
[3] For a review, see P. N. Pusey, in *Liquids, Freezing and the Glass Transition*, edited by J. P. Hansen, D. Levesque, and J. Zinn-Justin (North Holland, Amsterdam, 1991).
[4] A. van Blaaderen, R. Ruel, and P. Wiltzius, Nature (London) **385**, 321 (1997).
[5] A. van Blaaderen, Prog. Colloid Polym. Sci. **104**, 59 (1997).
[6] A. van Blaaderen and P. Wiltzius, Adv. Mater. **9**, 833 (1997).
[7] J. A. Barker and D. Henderson, Rev. Mod. Phys. **48**, 587 (1976).
[8] See, e.g., J. P. Hansen and I. R. McDonald, *Theory of Simple Liquids*, 2nd ed. (Academic Press, London, 1986).
[9] H. Löwen, Phys. Rep. **237**, 249 (1994).
[10] R. Evans in *Liquids at Interfaces, Les Houches Session XLVIII*, edited by J. Charvolin, J. F. Joanny, and J. Zinn-Justin (Elsevier, Amsterdam, 1990), p. 1ff.
[11] J. R. Henderson and F. van Swol, Mol. Phys. **51**, 991 (1984).
[12] D. Frenkel and B. Smit, *Understanding Molecular Simulation* (Academic, San Diego, 1996).
[13] R. Ohnesorge, H. Löwen, and H. Wagner, Phys. Rev. E **50**, 4801 (1994).
[14] B. Götzelmann, A. Haase, and S. Dietrich, Phys. Rev. E **53**, 3456 (1996).
[15] H. Reiss, H. L. Frisch, E. Helfand, and J. L. Lebowitz, J. Chem. Phys. **32**, 119 (1960).
[16] D. Henderson and M. Plischke, Proc. R. Soc. London, Ser. A **410**, 409 (1987).
[17] For a review, see Y. Rosenfeld, Mol. Phys. **94**, 929 (1998); see also Y. Rosenfeld, M. Schmidt, H. Löwen, and P. Tarazona, J. Phys.: Condens. Matter **8**, L577 (1996); Phys. Rev. E **55**, 4245 (1997).
[18] W. G. Hoover and F. H. Ree, J. Chem. Phys. **49**, 3609 (1968).
[19] P. G. Bolhuis, D. Frenkel, S.-C. Mau, and D. A. Huse, Nature (London) **388**, 235 (1997).
[20] See, e.g., M. P. Allen and D. J. Tildesley, *Computer Simulation of Liquids* (Clarendon Press, Oxford, 1989).
[21] *Observation, Prediction and Simulation of Phase Transitions in Complex Fluids* edited by M. Baus, L. F. Rull, and J. P. Ryckaert (Kluwer, Dordrecht, 1995).
[22] N. F. Carnahan and K. E. Starling, J. Chem. Phys. **51**, 635 (1969).
[23] D. J. Courtemanche and F. van Swol, Phys. Rev. Lett. **69**, 2078 (1992).
[24] J. G. Kirkwood, J. Chem. Phys. **18**, 380 (1950); W. W. Wood, *ibid.* **20**, 1334 (1952).
[25] K. J. Runge and G. V. Chester, Phys. Rev. A **36**, 4852 (1987).
[26] M. Schmidt and H. Löwen, Phys. Rev. Lett. **76**, 4552 (1996); Phys. Rev. E **55**, 7228 (1997).
[27] A. Münster, *Statistical Thermodynamics* (Springer, Berlin, 1974).
[28] Equivalently this can be deduced from the principle of maximization of entropy.
[29] A. C. Mitus, H. Weber, and D. Marx, Phys. Rev. E **55**, 6855 (1997).
[30] R. Ohnesorge, H. Löwen, and H. Wagner, Europhys. Lett. **22**, 245 (1993).
[31] D. W. M. Marr, J. Chem. Phys. **102**, 8283 (1995).
[32] A. Vrij, M. H. G. M. Penders, P. W. Rouw, C. G. de Kruif, J. K. G. Dhont, C. Smits, and H. N. W. Lekkerkerker, Faraday Discuss. Chem. Soc. **90**, 1 (1990).
[33] D. W. Marr and A. P. Gast, Langmuir **10**, 1348 (1994).
[34] B. J. Ackerson and K. Schätzel, Phys. Rev. E **52**, 6448 (1995).
[35] A. Mori, R. Manabe, and K. Nishioka, Phys. Rev. E **51**, R3831 (1995).
[36] A. Kyrlidis and R. A. Brown, Phys. Rev. E **51**, 5832 (1995).
[37] R. L. Davidchack and B. B. Laird, J. Chem. Phys. **108**, 9452 (1998).
[38] M. Schoen and S. Dietrich, Phys. Rev. E **56**, 499 (1997).
[39] A. Jaster, Europhys. Lett. **42**, 277 (1998); Phys. Rev. E **59**, 2594 (1999).
[40] J. W. M. Frenken and P. Stoltze, Phys. Rev. Lett. **82**, 3500 (1999).
[41] M. R. Maaroufi, A. Stipp, and T. Palberg, Prog. Colloid Polym. Sci. **11**, 83 (1998).
[42] S. Pronk and D. Frenkel, J. Chem. Phys. **110**, 4589 (1999).